

PACS numbers: 42.81.Dp; 78.60.Lc
DOI: 10.1070/QE2012v042n04ABEH014816

Optical properties of IR-emitting centres in Pb-doped silica fibres

A.S. Zlenko, S.V. Firstov, K.E. Riumkin, V.F. Khopin,
L.D. Iskhakova, S.L. Semjonov, I.A. Bufetov, E.M. Dianov

Abstract. **The first fibre preforms with a Pb-doped silica core, free of other dopants, have been produced using chemical vapour deposition. The preforms have been used to fabricate holey optical fibres. The spectroscopic properties of the fibres have been studied in detail in the range 400–1700 nm: we have measured the optical loss, constructed a three-dimensional luminescence excitation–emission graph and determined the decay time for the major luminescence peaks.**

Keywords: *lead, bismuth, fibre, luminescence, active centre, silica glass.*

1. Introduction

The engineering of laser materials is a priority issue in materials research and quantum electronics. In the last decade, significant advances have been made in the development of a radically new laser material: optical fibre based on bismuth-doped silica glass. After the discovery in 1999–2001 of IR luminescence in bismuth-doped glasses [1, 2], fabrication of the first bismuth-doped optical fibres [3] and demonstration of the first bismuth-doped fibre laser [4], a family of bismuth-doped fibre lasers operating in the range 1150–1550 nm have been created by varying the fibre core glass composition [5]. The efficiency of such lasers in some spectral ranges approaches 50% [6, 7]. In addition, bismuth-doped fibres were used to build fibre amplifiers that allowed the frequency range of optical fibre communication systems to be considerably extended [8, 9].

Unfortunately, there is a serious impediment to improving the performance of bismuth-doped fibre lasers and amplifiers: the lack of an appropriate model for IR-emitting bismuth centres in optical materials. Even though several models of IR-emitting centres have been proposed to date, which consider bismuth in a particular state in glass (e.g. Bi^{5+} [2, 10], Bi^{+} [11–14], Bi_2^{-}, Bi_2^{2-} and Bi_2/Bi_2^{2-} [15, 16]; a more detailed list can be found in Ref. [17]), none of them is supported by sufficient experimental evidence. A different approach was proposed by Sharonov et al. [18], who found that under certain experimental conditions Pb-, Sn- and Sb-doped aluminogermanate glasses exhibited IR luminescence that had roughly the same spectrum as that of bismuth-doped glasses. This finding led them to assume that the IR luminescence was due to defects in the glass network, independent of the nature of the dopant. It is worth noting that, according to their experimental data [18], the IR luminescence spectra of the Bi-, Pb-, Sn- and Sb-doped aluminogermanate glasses were indeed very similar to each other. Dianov [19] proposed that the bismuth centres in glass should be regarded as analogues of active centres in, e.g., alkali halide crystals doped with thallium and lead. The role of an active centre in such crystals is played by one or two thallium (or lead) atoms in a certain valence state on the cation site together with two or one adjacent vacancy. If the IR-emitting bismuth centres in silica-based glass are analogues of such centres in crystals, the active centre in glass should consist of one or two dopant atoms and a structural defect analogous to an anion vacancy. The most likely analogue of an anion vacancy in silica glass is a structural defect known as an oxygen-deficient centre.

IR luminescence in Pb-doped germanosilicate fibres was studied earlier by Bufetov et al. [20], who found that Pb- and Bi-doped germanosilicate fibres differed markedly in luminescence properties (in contrast to the Bi- and Pb-doped aluminogermanate glasses studied by Sharonov et al. [18]). The observed distinctions can be accounted for by a variety of factors, in particular by differences in glass composition and sample preparation procedure [18, 20] and differences in chemical properties between bismuth and lead. On the other hand, the spectra of Pb and Bi would be expected to coincide (like in Ref. [18]) when the Pb and Bi ions have isoelectronic configurations (e.g. Pb^{+} and Bi^{2+}). Therefore, one possible reason for the distinctions observed by Bufetov et al. [20] is that the Pb and Bi ions in the materials studied by them differed in electronic structure.

There is experimental evidence [21, 22] that the clearest to interpret results can be obtained for fibres of the simplest composition, e.g. those having a SiO_2 + Bi glass core (SBi fibre). It is of interest to directly compare the luminescence properties of bismuth and lead in fibres having a core from pure silica doped with these elements. Given this, the objectives of this work were to (1) produce a fibre with a pure silica core doped with Pb (SPb fibre), (2) study its optical properties and (3) compare the SPb fibre to a pure silica fibre doped with Bi (described in Refs [21, 22]) and silica fibre doped with lead and germanium (GSPb fibre) in order to assess the effect of germanium doping on the optical properties of the SPb fibre.

A.S. Zlenko, S.V. Firstov, K.E. Riumkin, L.D. Iskhakova, S.L. Semjonov, I.A. Bufetov, E.M. Dianov Fiber Optics Research Center, Russian Academy of Sciences, ul. Vavilova 38, 119333 Moscow, Russia; e-mail: aszlenko@fo.gpi.ru, fir@fo.gpi.ru, iabuf@fo.gpi.ru;
V.F. Khopin G.G. Devyatykh Institute of Chemistry of High-Purity Substances, Russian Academy of Sciences, ul. Tropinina 49, 603950 Nizhnii Novgorod, Russia; e-mail: vkhopin@mail.ru

Received 20 January 2012
Kvantovaya Elektronika **42** (4) 310–314 (2012)
Translated by O.M. Tsarev

2. Preform and fibre fabrication

A Pb-doped fibre preform, free of other dopants, was fabricated by the furnace chemical vapour deposition (FCVD) process [23, 24] (a modification of MCVD that employs a movable electric furnace, instead of an oxygen–hydrogen burner, to heat a section of a silica substrate tube). A porous layer of pure SiO_2 was deposited onto the inner surface of a silica substrate tube and then doped through impregnation with a Pb salt solution. The solution was prepared by dissolving metallic Pb in nitric acid:

$$3Pb + 8HNO_3 \rightarrow 3Pb(NO_3)_2 + 2NO\uparrow + 4H_2O.$$

The starting chemicals used were of extrapure grade. After the solution doping, the porous layer was dried and then sintered at ~1900 °C. Next, the silica tube was collapsed at ~2100 °C. The Pb concentration in the preform core was below the detection limit of our analytical facilities (0.02 at %), like in most such experiments with bismuth [5]. Because this low doping level cannot have a significant influence on the refractive index of the core, the reflective cladding was made in the form of a ring of six holes drilled in the preform. Next, the preform was drawn into fibre (whose cross section is shown in Fig. 1) while passing argon through the holes. The cladding diameter was 125 μm, and the average core diameter was about 10 μm. With this core diameter, the fibre was multimode.

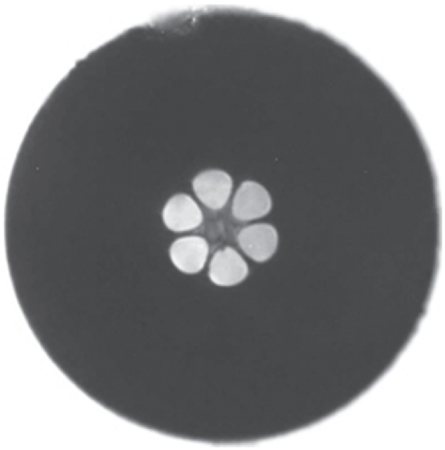

Figure 1. Cross-sectional photograph of the SPb fibre.

Pb-doped germanosilicate fibre was produced by the standard MCVD technique. A porous layer was also deposited onto the inner surface of a substrate tube, but its composition was 95 mol% SiO_2 + 5 mol% GeO_2. The layer was doped with Pb in the same way as above: through impregnation with a lead nitrate solution. Detailed information about this fibre can be found in Ref. [20].

3. Fibre characterisation techniques

The optical loss in the fibres was measured by the cut-back technique: by comparing the transmission of different lengths of the fibre (from several centimetres to 10 m). The luminescence of the core was recorded through the lateral surface of the fibre (to rule out the influence of reabsorption). Luminescence spectra were measured at various excitation wavelengths using an SC450 supercontinuum source (Fianium). Narrow-band ($\Delta\lambda$ = 3 nm) radiation (λ_{ex}) was separated out from the broad spectrum by an acousto-optic filter and was coupled into the fibre core. In all our measurements, the launched power was within 1 mW. Luminescence spectra were measured with an HP70950B spectrum analyser in the range λ_{em} = 875–1700 nm and with an Ocean Optics SP2000 spectrometer in the range 450–875 nm. In this way, we obtained luminescence spectra of the SPb fibre with λ_{ex} varied from 450 to 1700 nm in 10-nm steps. For comparison, we measured $I_{lum}(\lambda_{ex}, \lambda_{em})$ for the Pb-doped germanosilicate fibre in the ranges λ_{ex} = 600–1500 nm and λ_{em} = 770–1700 nm. The step in λ_{ex} determined the accuracy in the measured position of $I_{lum}(\lambda_{ex}, \lambda_{ex})$ peaks. The luminescence spectra were corrected for the spectral response of the measuring channel and normalised to the excitation power coupled into the fibre. All the measurements were made at room temperature.

Weak luminescence bands were examined using higher power excitation sources: frequency-doubled solid-state neodymium lasers (fundamental frequencies of 914 and 1064 nm), a He–Ne laser (633 nm), single-mode laser diodes (808, 975 and 1310 nm) and an ytterbium fibre laser (1058 nm). With these sources, the excitation power was tens of milliwatts.

4. Results and discussion

Figure 2 shows the optical loss spectra of the SPb and GSPb fibres. Since the fibres differ markedly in optical losses in the spectral range under consideration, their spectra have different vertical scales.

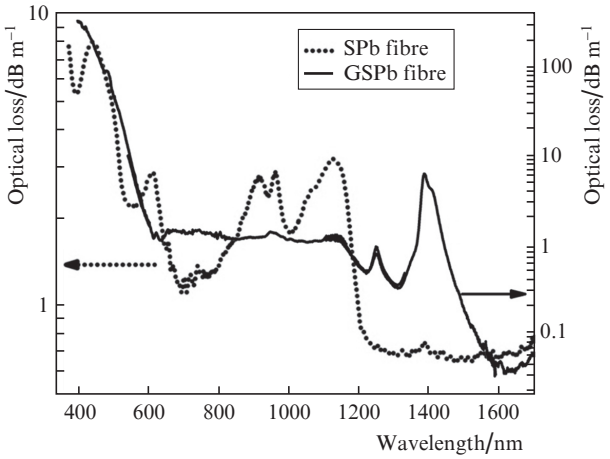

Figure 2. Optical loss spectra of the SPb and GSPb fibres.

The optical loss spectrum of the SPb fibre contains a broad IR absorption band centred at ~1130 nm, with a peak loss of 3.2 dB m^{-1}, which seems to be due to Pb-related IR centres. At wavelengths under 1 μm, there are loss peaks at 438, 606, 910 and 960 nm and a local minimum near 400 nm. Note that a similar minimum is present in the spectra of SBi fibres fabricated by different techniques [24–26].

The optical loss spectrum of the GSPb fibre differs significantly from that of the SPb fibre. First, it contains strong absorption peaks at 1.24, 1.38 and 1.41 μm, which points to

an appreciable concentration of OH groups (and can be accounted for by the specifics of the fibre fabrication process). Second, there are no prominent absorption peaks in the range 600–1150 nm. Finally, in the short-wavelength region (λ < 600 nm) the optical loss rises steeply (by two orders of magnitude). Thus, the spectrum of the SPb fibre has considerably more characteristic features in comparison with that of the GSPb fibre.

The luminescence spectra measured in a broad wavelength range, in combination with a stepwise variation in excitation wavelength, allowed us to obtain $I_{lum}(\lambda_{ex}, \lambda_{em})$ distributions for the SPb and GSPb fibres (Fig. 3). The distributions have the form of grey-scale contours that represent both luminescence spectra (along the horizontal axis) and excitation spectra (along the vertical axis).

In these distributions, the ratio of the maximum to minimum I_{lum} value is ~100, which limits the represented information (at low luminescence intensities). Without such limitation, however, three-dimensional (3D) luminescence graphs are essentially unreadable, so it should be kept in mind that they show only the major observed luminescence peaks.

The designations of the observed luminescence peaks in the $I_{lum}(\lambda_{ex}, \lambda_{em})$ distributions and the corresponding excitation and emission wavelengths are listed in Table 1. In what follows, the luminescence peaks will be denoted like in Table 1 (or Fig. 3) in combination with the corresponding excitation and emission wavelengths, e.g. A ($\lambda_{ex}^{max}, \lambda_{em}^{max}$)

Table 1. Excitation and luminescence wavelengths and designations of the major luminescence peaks of the SPb and GSPb fibres.

Fibre	Luminescence band	λ_{ex}^{max}/nm	λ_{em}^{max}/nm
SPb	A	1100	1145
SPb	A1	450	1145
SPb	B	930	1400
GSPb	AG	1140	1155
GSPb	BG	947	1011
GSPb	CG	<450	670
GSPb	DG	510	1240

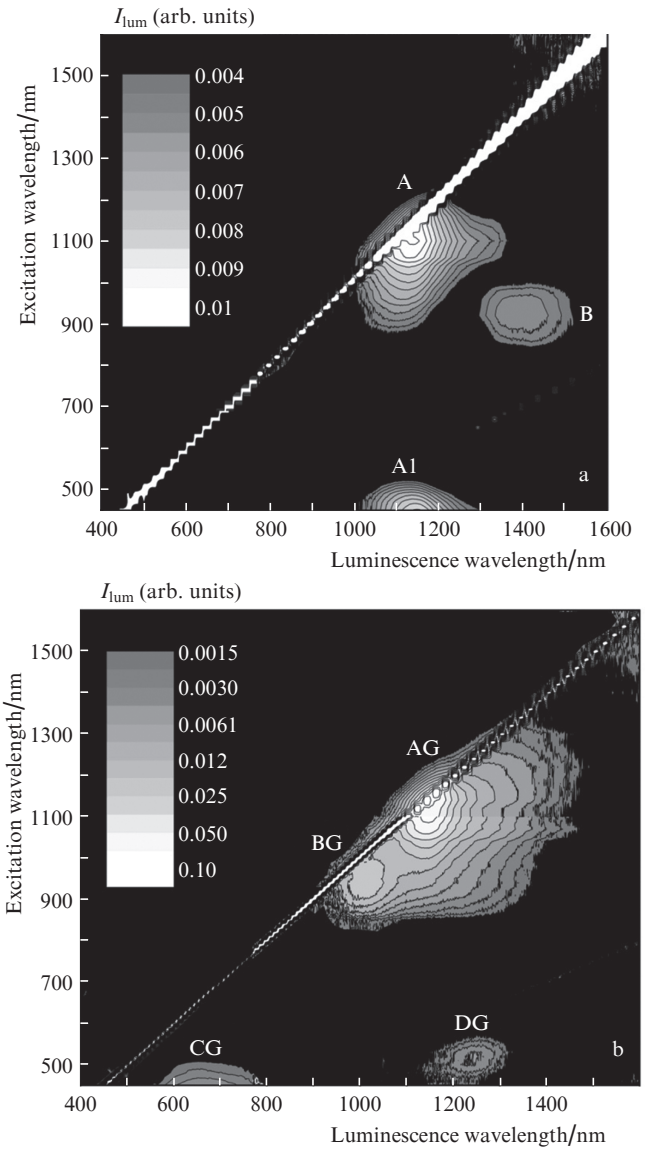

Figure 3. Luminescence intensity as a function of luminescence and excitation wavelengths for the (a) SPb and (b) GSPb fibres.

The luminescence spectra of both fibres show a number of peaks, some of which have a complex shape and overlap. The width of the luminescence peaks in the $I_{lum}(\lambda_{ex}, \lambda_{ex})$ distributions reaches ~100 nm or even more. The $\lambda_{em} = \lambda_{ex}$ diagonal across the two $I_{lum}(\lambda_{ex}, \lambda_{ex})$ graphs represents the scattered excitation radiation. Also shown is the second-order diffraction of the scattered excitation radiation in the form of a portion of the $\lambda_{em} = 2\lambda_{ex}$ line.

The excitation–luminescence spectrum of the SPb fibre (Fig. 3a) has only three major luminescence peaks: A, A1 and B (Table 1). The luminescence regions are asymmetric in shape (especially region A), which indicates that they have a complex structure. Bands A and A1, resulting from excitation at different wavelengths, differ very little in luminescence wavelength, which suggests that they are due to the same active centre.

The excitation–luminescence spectrum of the GSPb fibre (Fig. 3b) differs markedly from that of the SPb fibre. It contains the red luminescence band CG (450 nm, 670 nm), which has no analogue in Fig. 3a, and two new luminescence bands, DG and BG. Moreover, there is no 1400-nm luminescence (no analogue of band B in Fig. 3a). At the same time, the strongest luminescence bands of the SPb and GSPb fibres (A in Fig. 3a and AG in Fig. 3b) differ little in excitation and luminescence wavelengths.

Figure 4 shows luminescence spectra of the SPb fibre at a higher pump power (several tens of milliwatts). In contrast to that in Fig. 3, the luminescence intensity in Fig. 4 has different scales for each curve. Note that, at an excitation wavelength of 1310 nm, no luminescence was detected in the spectral region studied.

When the SPb fibre was excited with various intensities at the six wavelengths indicated in Fig. 4, we observed luminescence near 1145 nm. This corresponds to the luminescence in different sections of regions A and A1 in Fig. 3a. Because of the asymmetry of these regions, the peak-emission wavelengths slightly vary with excitation wavelength. In particular, under excitation at 457, 532, 633, 808, 975 and 1058 nm the peak-emission wavelength is 1145, 1125, 1120, 1090, 1125 and 1145 nm, respectively.

At excitation wavelengths of 532, 633 and 808 nm, there is also luminescence at 880, 870 and 875 nm, respectively, which is not seen in Fig. 3a because of its relatively low intensity.

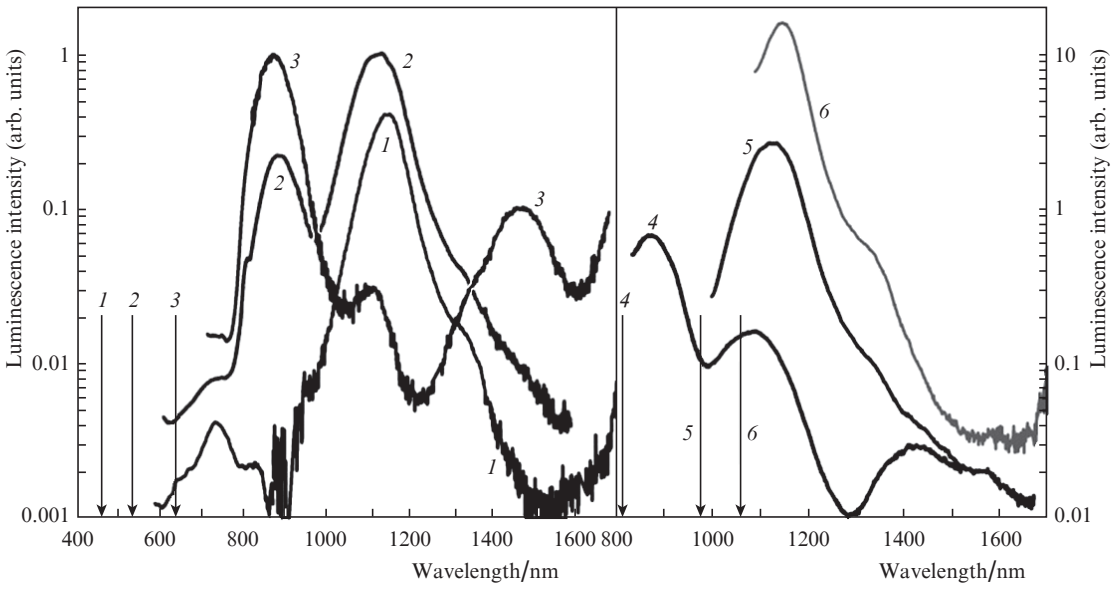

Figure 4. Luminescence spectra of the SPb fibre at excitation wavelengths λ_{ex} = (*1*) 457, (*2*) 532, (*3*) 633, (*4*) 808, (*5*) 975 and (*6*) 1058 nm. The numbered arrows indicate the excitation wavelengths.

Moreover, at λ_{ex} = 633 and 808 nm we observe luminescence at λ_{em}^{max} = 1464 and 1428 nm, which is assignable to region B in Fig. 3a. That the intensity of the 1400-nm luminescence, observed at an increased excitation density, is lower than that of the 870-nm luminescence, which is not seen in Fig. 3a, can be accounted for by the fact that the shape of the luminescence spectrum depends on excitation intensity, as occurs in a number of cases for Bi-doped fibres [27].

In several luminescence spectra, the band centred around 1145 nm has a shoulder near 1330 nm, which is about an order of magnitude weaker than the luminescence peak at λ_{em}^{max} = 1145 nm.

It should be emphasised that pumping at 457, 975 and 1058 nm excites mostly the 1145-nm luminescence, whereas excitation at 532, 633 and 808 nm gives rise to luminescence bands at 870 and 1450 nm (Figs 3a, 4). It is therefore reasonable to assume that the SPb fibre contains at least two types of active centres. One centre (which will be referred to as type 1) is responsible for the 600-nm absorption and the luminescence bands at 870 and 1450 nm, and the other (type 2) is responsible for the 1150-nm luminescence band and 1100-nm absorption band. In SBi fibres, only one IR-emitting bismuth centre has been identified to date [21, 22] (in addition to the red luminescence of Bi^{2+}), and no luminescence bands attributable to any other IR-emitting centres were detected in measurements of 3D luminescence excitation–emission spectra [7, 21] or at increased luminescence excitation intensities [26] (measurements analogous to those in this study).

We also studied the luminescence decay kinetics in the SPb fibre at different excitation wavelengths for the bands centred at 1150 (type 2 centre) and 870 nm (type 1). In all cases, the luminescence decay was well represented by a single exponential, with a decay time τ_A = 650 μs for the 1150-nm luminescence and τ_D = 30 μs for the 870-nm luminescence. The decay of the luminescence between 1100 and 1300 nm in the GSPb fibre comprises two exponential components, comparable in intensity. The shorter decay time is 4.5 μs and the longer one is 40 μs. Thus, doping with germanium modifies the luminescence spectrum of the SPb fibre, having little effect on the major peak in the IR spectral region and slightly reducing the luminescence decay time.

5. Conclusions

An optical fibre with a Pb-doped pure silica core has been fabricated for the first time and its optical properties have been studied. 3D excitation–emission spectra of SPb and GSPb fibres have been obtained for the first time. The results demonstrate that the major IR luminescence peak of the SPb fibre is located near 1150 nm. The lifetime of this luminescence, near 60 μs, is about one order of magnitude shorter than that in bismuth-doped fibre of the same composition. The SPb fibre is shown to contain two IR-emitting centres differing in excitation and luminescence spectra. In contrast to aluminogermanate glasses, which have very similar luminescence spectra when doped with Bi and Pb [18], the fibres with pure silica or germanosilicate glass cores differ markedly in luminescence properties, which poses new questions regarding the search for an appropriate physical model of IR-emitting centres.

References

1. Murata K., Fujimoto Y., Kanabe T., Fujita H., Nakatsuka M. *Fusion Eng. Des.*, **44**, 437 (1999).
2. Fujimoto Y., Nakatsuka M. *Jpn. J. Appl. Phys.*, **40**, L279 (2001).
3. Dvoyrin V.V., Mashinsky V.M., Dianov E.M., Umnikov A.A., Yashkov M.V., Guryanov A.N. *Proc. Europ. Conf. Opt. Commun.* (Glasgow, UK, 2005) paper Th 3.3.5.
4. Dianov E.M., Dvoyrin V.V., Mashinskii V.M., Umnikov A.A., Yashkov M.V., Gur'yanov A.N. *Kvantovaya Elektron.*, **35**, 1083 (2005) [*Quantum Electron.*, **35**, 1083 (2005)].
5. Bufetov I.A., Dianov E.M. *Laser Phys. Lett.*, **6**, 487 (2009).
6. Bufetov I.A., Melkumov M.A., Khopin V.F., Firstov S.V., Shubin A.V., Medvedkov O.I., Guryanov A.N., Dianov E.M. *Proc. SPIE Int. Soc. Opt. Eng.*, **7580**, 758014 (2010).
7. Firstov S.V., Shubin A.V., Khopin V.F., Mel'kumov M.A., Bufetov I.A., Medvedkov O.I., Gur'yanov A.N., Dianov E.M. *Kvantovaya Elektron.*, **41**, 581 (2011) [*Quantum Electron.*, **41**, 581 (2011)].

8. Melkumov M.A., Bufetov I.A., Shubin A.V., Firstov S.V., Khopin V.F., Guryanov A.N., Dianov E.M. *Opt. Lett*., **36,** 2408 (2011).
9. Dianov E.M., Mel'kumov M.A., Shubin A.V., Firstov S.V., Khopin V.F., Gur'yanov A.N., Bufetov I.A. *Kvantovaya Elektron*., **39**, 1099 (2009) [*Quantum Electron*., **39**, 1099 (2009)].
10. Ohkura T., Fujimoto Y., Nakatsuka M., Young-Seok S. *J. Am. Ceram. Soc*., **90**, 3596 (2007).
11. Peng M.Y., Qiu J.R., Chen D.P., Meng X.G., Zhu C.S. *Opt. Lett*., **30** (18), 2433 (2005).
12. Qiu Y.Q., Shen Y.H. *Opt. Mater*., **31** (2), 223 (2008).
13. Dvoyrin V.V., Mashinsky V.M., Bulatov L.I., Bufetov I.A., Shubin A.V., Melkumov M.A., Kustov E.F., Dianov E.M., Umnikov A.A., Khopin V.F., Yashkov M.V., Guryanov A.N. *Opt. Lett*., **31**, 2966 (2006).
14. Truong V.G., Bigot L., Lerouge A., Douay M., Razdobreev I. *Appl. Phys. Lett*., **92**, 041908 (2008).
15. Khonton S., Morimoto S., Arai Y., Ohishi Y. *Suranaree J. Sci. Technol*., **14**, 141(2007).
16. Sokolov V.O., Plotnichenko V.G., Dianov E.M. *Opt. Lett*., **33**, 1488 (2008).
17. Peng M., Dong G., Wondraczec L., Zhang L., Zhang N., Qiu J. *J. Non-Cryst. Solids*, **357**, 2241 (2011).
18. Sharonov M.Yu., Bykov A.B., Petricevic V., Alfano R.R. *Opt. Lett*., **33**, 2131 (2008).
19. Dianov E.M. *Kvantovaya Elektron*., **40**, 283 (2010) [*Quantum Electron*., **40**, 283 (2010)].
20. Bufetov I.A., Firstov S.V., Khopin V.F., Abramov A.N., Guryanov A.N., Dianov E.M. *Opt. Express*, **17**, 13487 (2009).
21. Firstov S.V., Khopin V.F., Bufetov I.A., Firstova E.G., Guryanov A.N., Dianov E.M. *Opt. Express*, **19**, 19551 (2011).
22. Bufetov I.A., Melkumov M.A., Firstov S.A., Shubin A.V., Semenov S.L., Vel'miskin V.V., Levchenko A.E., Firstova E.G., Dianov E.M. *Opt. Lett*., **36**, 166 (2011).
23. Malinin A.A., Zlenko A.S., Akhmetshin U.G., Semjonov S.L. *Proc. SPIE Int. Soc. Opt. Eng*., **7934**, 793418 (2011).
24. Zlenko A.S., Dvoyrin V.V., Mashinsky V.M., Denisov A.N., Iskhakova L.D., Mayorova M.S., Medvedkov O.I., Semenov S.L., Vasiliev S.A., Dianov E.M. *Opt. Lett*., **36**, 2599 (2011).
25. Razdobreev I., El Hamzaoui H., Ivanov V.Yu., Kustov E.F., Capoen B., Bouazaoui M. *Opt. Lett.*, **35**, 1341 (2011).
26. Bufetov I.A., Semenov S.L., Vel'miskin V.V., Firstov S.V., Bufetova G.A., Dianov E.M. *Kvantovaya Elektron*., **40**, 639 (2010) [*Quantum Electron*., **40**, 639 (2010)].
27. Dianov E.M., Firstov S.V., Khopin V.F., Medvedkov O.I., Gur'yanov A.N., Bufetov I.A. *Kvantovaya Elektron*., **39**, 299 (2009) [*Quantum Electron*., **39**, 299 (2009)].